CANCER

Cysteine depletion induces pancreatic tumor ferroptosis in mice

Michael A. Badgley[1,2]*, Daniel M. Kremer[3,4]†, H. Carlo Maurer[1,2,5]†, Kathleen E. DelGiorno[6], Ho-Joon Lee[3,4], Vinee Purohit[3,4], Irina R. Sagalovskiy[1,2], Alice Ma[1,2], Jonathan Kapilian[1,2], Christina E. M. Firl[1,2], Amanda R. Decker[1,2], Steve A. Sastra[1,2], Carmine F. Palermo[1,2], Leonardo R. Andrade[7], Peter Sajjakulnukit[3,4], Li Zhang[4,8], Zachary P. Tolstyka[3,4], Tal Hirschhorn[9], Candice Lamb[10], Tong Liu[2,11,12], Wei Gu[2,11,12], E. Scott Seeley[13,14], Everett Stone[10,15], George Georgiou[15], Uri Manor[7], Alina Iuga[2,12], Geoffrey M. Wahl[6], Brent R. Stockwell[9], Costas A. Lyssiotis[3,4,16], Kenneth P. Olive[1,2]‡

Ferroptosis is a form of cell death that results from the catastrophic accumulation of lipid reactive oxygen species (ROS). Oncogenic signaling elevates lipid ROS production in many tumor types and is counteracted by metabolites that are derived from the amino acid cysteine. In this work, we show that the import of oxidized cysteine (cystine) via system x_C^- is a critical dependency of pancreatic ductal adenocarcinoma (PDAC), which is a leading cause of cancer mortality. PDAC cells used cysteine to synthesize glutathione and coenzyme A, which, together, down-regulated ferroptosis. Studying genetically engineered mice, we found that the deletion of a system x_C^- subunit, *Slc7a11*, induced tumor-selective ferroptosis and inhibited PDAC growth. This was replicated through the administration of cyst(e)inase, a drug that depletes cysteine and cystine, demonstrating a translatable means to induce ferroptosis in PDAC.

Pancreatic ductal adenocarcinoma (PDAC) is a deadly cancer that is resistant to traditional therapies. More than 90% of PDAC cases harbor mutations in *KRAS* that both promote proliferation and alter cellular metabolism. A by-product of mutant-KRAS signaling is the increased production of reactive oxygen species (ROS), which can damage cellular components. To compensate, PDAC cells up-regulate metabolic programs that detoxify ROS using cysteine-derived metabolites such as glutathione (GSH) (*1*). Most cellular cysteine is acquired through the system x_C^- antiporter, which exchanges extracellular, oxidized cysteine (cystine) for intracellular glutamate. Yet, germline deletion of the system x_C^- gene, *Slc7a11*, is well tolerated in unstressed mice (*2*), which suggests that normal cells have low basal cystine import requirements. We hypothesized that cystine import is a critical dependency of PDAC that may be selectively targeted as an anticancer therapy.

To investigate the role of cysteine metabolism in PDAC, we measured the viability of human PDAC cell lines cultured for 24 hours in media with varying concentrations of cystine or the system x_C^- inhibitor imidazole ketone erastin (IKE) (Fig. 1, A and B) (*3*). In four of five PDAC lines, cystine starvation reduced cell viability by >80%; this was largely prevented by addition of the lipophilic antioxidant Trolox. Cystine-starved cells underwent catastrophic destabilization of their plasma membranes, without visual evidence of nuclear fragmentation (movie S1). IKE treatment mimicked the effects of cystine withdrawal, quickly killing most cells from the four sensitive PDAC lines in a manner that was visually identical to that of cystine starvation but distinct from staurosporine-induced apoptosis (fig. S1A and movies S2 and S3). Neither cystine starvation nor system x_c^- inhibition (collectively referred to as cysteine depletion) induced caspase 3 cleavage (fig. S1B), which indicates that the cell death was not apoptotic. Rather, the oxidative cell death resembled ferroptosis, a form of iron-dependent, non-apoptotic cell death previously associated with system x_C^- inhibition (*4*). We found that cotreatment of human PDAC cells with either deferoxamine (DFO, an iron chelator), ferrostatin-1 (Fer1, a ferroptosis inhibitor), or N-acetylcysteine (NAC, a cell-permeable analog of cysteine) markedly reduced cell death from cysteine depletion, whereas inhibitors of apoptosis or necroptosis had little impact on cell death, consistent with previous reports (Fig. 1C and fig. S1, C to E) (*5*). Autophagy inhibition had variable effects in different lines, likely reflecting the known effect of ferritinophagy on ferroptosis (*6*). Using the fluorescent probe C11-BODIPY, we observed a large increase in lipid oxidation (a hallmark of ferroptosis) prior to cell death in response to cysteine depletion; this was prevented by cotreatment with Trolox, Fer-1, NAC, and DFO (Fig. 1D and fig. S2, A and B). By contrast, elevated total ROS levels induced by cysteine depletion were not prevented by these agents, which argues against a more general oxidative process (fig. S2C). We conclude from these experiments that most PDAC lines rely on cysteine to prevent ferroptotic cell death. An analysis of *SLC7A11* expression across human datasets revealed a modest overexpression in PDAC versus normal tissues, enrichment in the malignant epithelial compartment of PDAC, and an association with signatures of redox stress (fig. S3). Across multiple human cancers, *SLC7A11* was frequently overexpressed and associated with reduced survival (fig. S4).

To learn whether pancreatic tumors in mice depend on system x_c^- for survival, we employed a dual recombinase genetic engineering strategy based on the KPC mouse model (*7*). $Kras^{FSF.G12D/+}$; $Tp53^{R172H/+}$; $Pdx1FlpO^{tg/+}$; $Slc7a11^{Fl/Fl}$; $Rosa26^{CreERT2/+}$ (KPFSR) mice (fig. S5) spontaneously develop PDAC driven by FlpO-dependent activation of mutant *Kras* and germline expression of mutant *Tp53*. These tumors are identical in genotype and phenotype to the KPC model, but the administration of tamoxifen induces systemic deletion of *Slc7a11* through the action of Cre recombinase expressed from the *Rosa26* locus (figs. S5 and S6, A to C). We randomized KPFSR mice bearing 4 to 7 mm tumors to receive six daily doses of vehicle or tamoxifen and monitored tumor growth by ultrasound (*8*). We found that deletion of *Slc7a11* in established tumors of KPFSR mice nearly doubled median survival compared with vehicle treatment (Fig. 2A; $P = 0.0295$, $n = 10$ per group). Most recombined tumors exhibited a period of stable disease or partial response—and one underwent a complete regression—but these responses were never observed in vehicle-treated mice (Fig. 2B and figs. S6, D to F, and S7A). Critically, the addition of NAC to the drinking water of tamoxifen-treated mice restored baseline survival and eliminated tumor responses, supporting a link to cysteine metabolism (Fig. 2, A and B). At

[1]Division of Digestive and Liver Diseases, Department of Medicine, Columbia University Medical Center, New York, NY 10032, USA. [2]Herbert Irving Comprehensive Cancer Center, Columbia University Medical Center, New York, NY 10032, USA. [3]Department of Molecular and Integrative Physiology, University of Michigan, Ann Arbor, MI 48109, USA. [4]Rogel Cancer Center, University of Michigan, Ann Arbor, MI 48109, USA. [5]Klinikum rechts der Isar, II, Medizinische Klinik, Technische Universität München, 81675, Munich, Germany. [6]Gene Expression Laboratory, Salk Institute for Biological Studies, La Jolla, CA 92037, USA. [7]Waitt Advanced Biophotonics Center, Salk Institute for Biological Studies, La Jolla, CA 92037, USA. [8]Michigan Regional Comprehensive Metabolomics Resource Core, University of Michigan, Ann Arbor, MI 48105, USA. [9]Departments of Biological Sciences and Chemistry, Columbia University, New York, NY 10027, USA. [10]Department of Chemical Engineering, University of Texas at Austin, Austin, TX 78712, USA. [11]Institute for Cancer Genetics, Columbia University Medical Center, New York, NY 10032, USA. [12]Department of Pathology, Columbia University Medical Center, New York, NY 10032, USA. [13]Department of Pathology, University of California, San Francisco, CA 94143, USA. [14]Salvo Therapeutics, San Francisco, CA 94117, USA. [15]Department of Molecular Biosciences, University of Texas at Austin, Austin, TX 78712, USA. [16]Department of Internal Medicine, Division of Gastroenterology, University of Michigan, Ann Arbor, MI 48109, USA.
*Present address: Department of Biochemistry and Molecular Pharmacology, Langone Medical Center, New York University, New York, NY 10016, USA. †These authors contributed equally to this work.
‡Corresponding author. Email: kenolive@columbia.edu

necropsy, escaped tumors exhibited evidence of incomplete *Slc7a11* recombination by polymerase chain reaction and restored protein expression by Western blotting, which suggests the outgrowth of unrecombined tumor cells (fig. S7, B and C).

The study of in vivo ferroptosis has been hindered by the lack of a validated, selective biomarker and the absence of a histopathological characterization of the phenomenon in tissues. Within tamoxifen-treated KPFSR tumors, we observed numerous lesions of ballooned epithelial cells with lipid droplet-like structures and intermittent megamitochondria, often juxtaposed to necrotic regions—a phenotype only occasionally observed in vehicle-treated KPFSR and untreated KPC tumors (Fig. 2, C and D, and fig. S7C). These lesions exhibited no alterations in apoptosis or proliferation markers (fig. S8, A and B), but they did display accumulation of 4-hydroxynonenal (4HN) (fig. S8, C to E), a by-product of lipid peroxidation, making them candidates for in vivo ferroptosis. Critically, no pathologies were observed in nonpancreatic tissues of tamoxifen-treated KPFSR mice, indicating a tumor-selective phenotype. Transmission electron microscopy (TEM) and Oil Red O staining of tamoxifen-treated KPFSR tumors confirmed the presence of abnormally large lipid droplets (Fig. 2D and fig. S8F). TEM also revealed structural aberrations in the mitochondria of malignant epithelial cells, including disrupted cristae and compromised membrane integrity (Fig. 2E), which is consistent with the results of prior in vitro studies (*9*). Finally, we performed laser capture microdissection and RNA sequencing to isolate malignant epithelial cells from KPFSR tumors. We found that genes up-regulated in response to *Slc7a11* deletion were enriched in a ferroptotic expression signature from erastin-treated HT-1080 cells (Fig. 2F) (*10*), whereas apoptotic gene sets were not enriched (table S1). We conclude that the phenotype observed in tamoxifen-treated KPFSR tumors is a histologically identifiable, in vivo manifestation of ferroptosis.

Prior studies have indicated that cysteine regulates ferroptosis primarily through the synthesis of GSH, a critical cofactor for the lipid peroxide–detoxifying enzyme GPX4 (*3*). We found that cysteine depletion rapidly reduced GSH levels in two human PDAC cell lines (fig. S9A). Furthermore, cotreatment with the membrane-permeable GSH analog glutathione ethyl ester prevented lipid oxidation and ferroptosis (fig. S9, B to E). However, inhibition of GSH biosynthesis using buthionine sulfoximine (BSO) (fig. S9F) did not induce lipid ROS or reduce cell viability (Fig. 3, A and B), which demonstrates that GSH loss is not sufficient to induce ferroptosis in PDAC cells (*11*). To investigate whether additional cysteine-derived metabolites contribute to the regulation of ferroptosis, we traced the metabolism of exogenous cystine by using ^{13}C-labeled cystine and measuring labeled metabolites by mass spectrometry. In addition to exhibiting rapid flux into GSH pools, cystine was also converted to coenzyme A (CoA) over 24 hours (Fig. 3 C and D); no flux was observed into taurine, lactate, citrate, or glutamate (fig. S9G). CoA is synthesized from cysteine via the pantothenate pathway and plays a role in many metabolic pathways, particularly lipid metabolism. Both CoA and its derivative coenzyme Q_{10} (CoQ_{10}) have been shown to affect sensitivity to ferroptosis (*12*, *13*). We found that system x_C^- inhibition reduced CoA levels and increased levels of pantothenate (Fig. 3E), a metabolite upstream of cysteine incorporation in CoA synthesis. Moreover, treatment of PDAC cells with exogenous CoA (*14*) prevented IKE-induced ferroptosis (Fig. 3F) whereas pantothenate kinase inhibition with PANKi sensitized cells to IKE (fig. S10, A to C). Notably, PANKi combined synergistically with BSO to induce ferroptosis (Fig. 3G and fig. S10D). Cotreatment with idebenone (a membrane-permeable analog of CoQ_{10}) or a monounsaturated fatty acid blocked BSO/PANKi-induced ferroptosis, whereas saturated or polyunsaturated fatty acids did not (fig. S10E), similar to prior observations with IKE (*15*). Together, these experiments demonstrate that CoA and GSH cooperate to regulate ferroptosis in human PDAC cells (fig. S10H).

Finally, we sought a pharmacological means to target cysteine metabolism in pancreatic tumors. Drug delivery is compromised in PDAC because of the effects of fibrosis on tissue perfusion (*16*). Although current system x_C^- inhibitors are not optimized for the PDAC microenvironment, the engineered enzyme cyst(e)inase is well-tolerated in mammals, has a long half-life, and potently degrades both cystine and cysteine in circulation (*17*). In vitro, cyst(e)inase treatment induced lipid oxidation and reduced the viability of IKE-sensitive PDAC lines; this was largely prevented by cotreatment with ferroptosis inhibitors (Fig. 4, A to C, and fig. S11, A and B). To determine the effects of cyst(e)inase on pancreatic tumors in vivo, we treated tumor-bearing KPC mice for

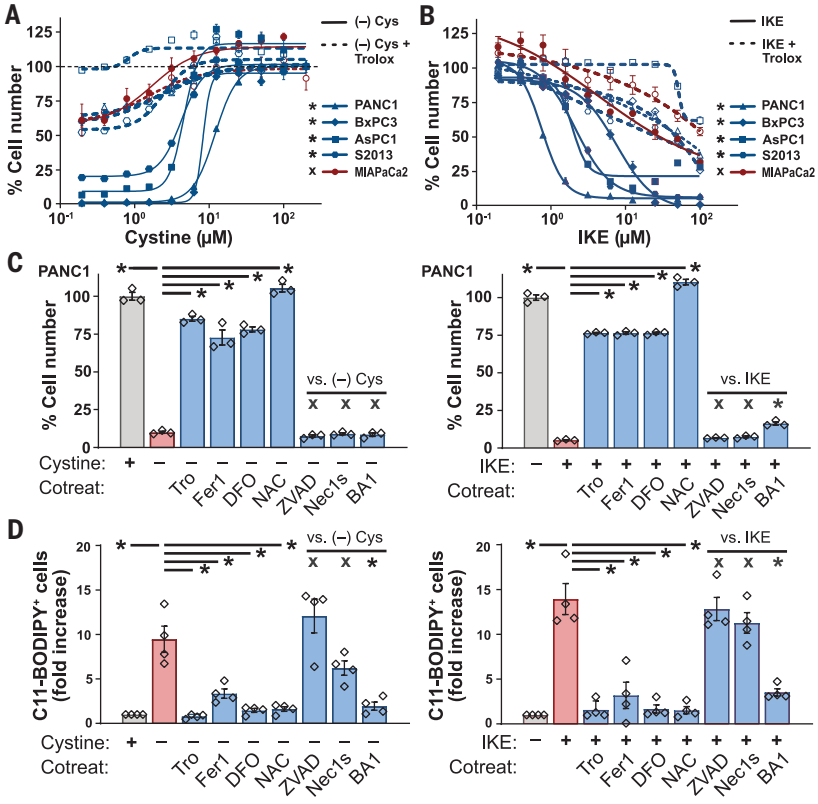

Fig. 1. Pancreatic cancer cells require exogenous cystine to avert ferroptosis. (**A** and **B**) Viability of human PDAC lines after 24 hours culture in varying concentrations of cystine (A) or IKE (B), alone or in combination with 100 μM Trolox. Student's *t* test was performed, comparing maximal cytotoxicity ± Trolox. (**C**) Viability of PANC-1 cells cultured for 24 hours in cystine-free media (left) or treated with 10 μM IKE (right), alone or in combination with 100 μM Trolox (Tro), 500 nM ferrostatin-1 (Fer1), 100 μM deferoxamine (DFO), 1mM N-acetyl cysteine (NAC), 50 μM ZVAD-FMK, 1 nM Bafilomycin A1 (BA1), or 10 μM Necrostatin-1s (Nec1s). Tukey test was performed. (**D**) Flow cytometry of C11-BODIPY fluorescence in PANC-1, AsPC-1, BxPC-3, and S-2013 cells after 6 to 8 hours of treatment with conditions from (C). Tukey test was performed. All data are means ± SEM of three independent experiments. *$P < 0.05$; x, no significant difference.

10 days with vehicle, low-dose cyst(e)inase, or high-dose cyst(e)inase (n = 2 for each treatment). Histopathological examination of cyst(e)inase-treated tumors revealed a severe ferroptosis phenotype, with extensive lipid droplet formation, stromal disruption, decompressed blood vessels, and necrosis (Fig. 4, D and E, and fig. S12, A and B). TEM revealed enlarged lipid droplet formation, extracellular lipid droplets, and mitochondrial defects, preferentially in cyst(e)inase-treated KPC tumors (Fig. 4, F to I). Ferroptotic lesions were generally 4HN positive and cleaved caspase 3 negative (fig. S13A). Finally, four additional KPC mice

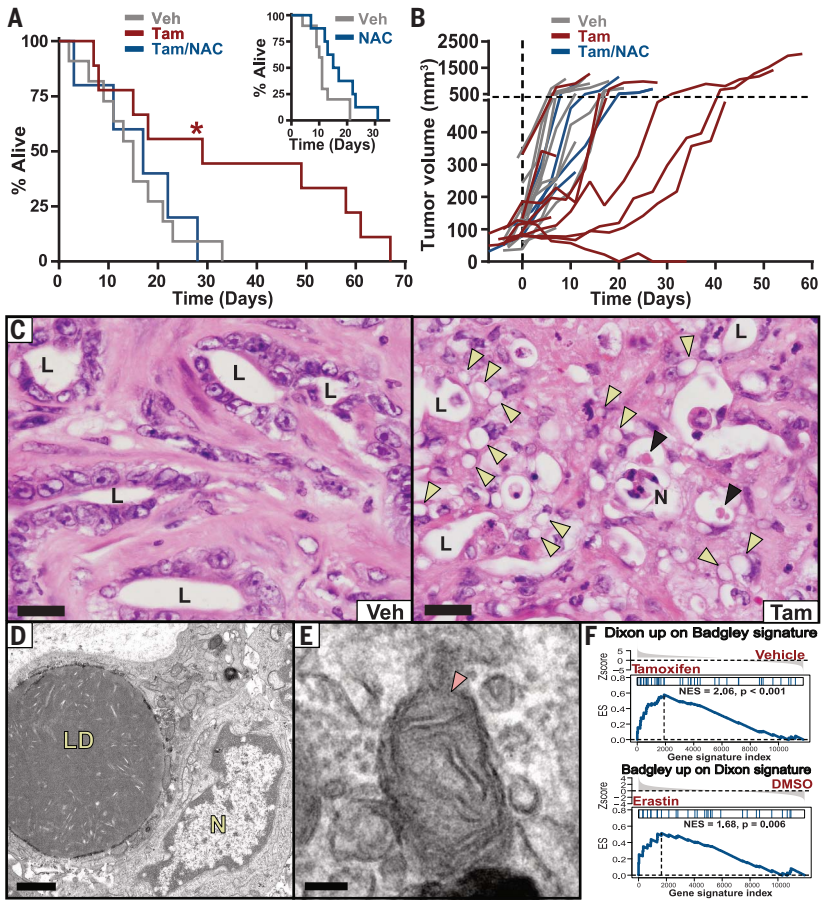

Fig. 2. Deletion of *Slc7a11* in KPC mice induces tumor ferroptosis and extends survival. (**A**) Survival of KPFSR mice treated with vehicle (Veh) (n = 11, median 15 days), tamoxifen (Tam) (n = 9, median 29 days), or tamoxifen/NAC (n = 5, median 17 days). *P < 0.0295, log-rank. Inset shows the survival of KPC mice treated with NAC alone (n = 8, median 16 days) versus historical saline-treated controls (n = 10, median 11 days). (**B**) Growth curves for each KPFSR tumor. (**C**) Hematoxylin and eosin (H&E)–stained sections of tumor tissue from KPFSR mice treated with vehicle (left) or tamoxifen (right). L, lumen of malignant epithelium; N, necrosis; yellow arrowheads, lipid droplets; black arrowheads, megamitochondria; scale bars, 20 μm. (**D** and **E**) TEM images from tamoxifen-treated KPFSR tumors. LD, lipid droplets; N, nucleus; arrowhead indicates damaged mitochondrion. Scale bar (D), 1μm; scale bar (E), 100 nm. (**F**) Gene set enrichment analysis. Top panel depicts enrichment of a published ferroptosis expression signature (Dixon) among genes differentially expressed in tamoxifen-treated KPFSR epithelia (Badgley) (P < 0.001). Bottom panel depicts the reciprocal comparison (P < 0.006). NES, normalized enrichment score; DMSO, dimethyl sulfoxide.

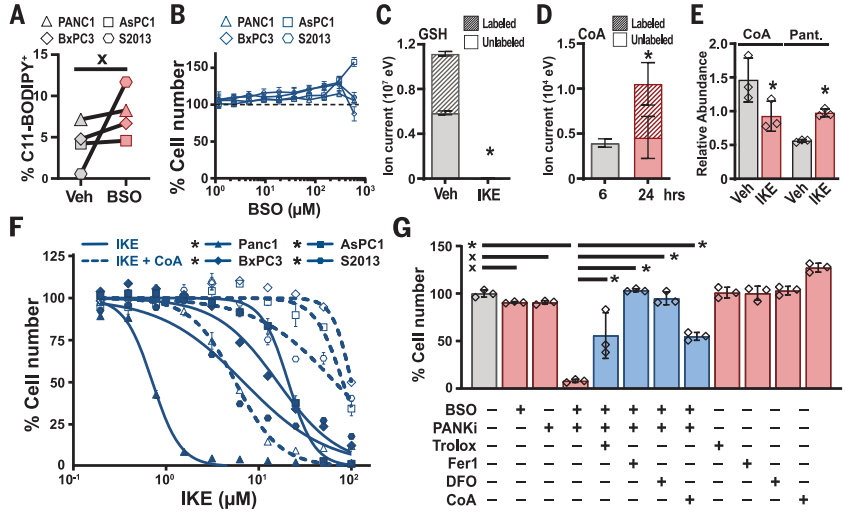

Fig. 3. Combination GSH and CoA inhibition induces ferroptosis in human PDAC cells. (**A**) Flow cytometry for C11-BODIPY fluorescence in four human PDAC lines treated for 6 hours with 150 μM BSO. Paired t test was performed. (**B**) Viability of human PDAC cells treated for 24 hours with indicated concentrations of BSO. (**C**) Liquid chromatography time-of-flight mass spectrometry (LC-TOF-MS) analysis of GSH in PANC-1 cells labeled for 6 hours with ^{13}C-cystine combined with vehicle or 5μM IKE. Student's t test was performed. (**D**) LC-TOF-MS analysis of CoA in PANC-1 cells labeled for 6 hours with ^{13}C-cystine, after 6 or 24 hours. Student's t test was performed. (**E**) Liquid chromatography triple quadrupole tandem mass spectrometry measurements of CoA and pantothenate (Pant.) levels in Panc-1 cells treated with vehicle and IKE for 6 hours. Student's t test was performed. (**F**) Viability of human PDAC cell lines treated with IKE, alone or in combination with 200 μM CoA. Student's t test comparing maximal cytotoxicity ± CoA was performed. (**G**) PANC-1 cells treated for 24 hours with combinations of 300 μM BSO and 5 μM PANKi along with Trolox, Fer-1, DFO, or CoA, as described in Fig. 1C. Tukey test was performed. In (A) to (G), *P < 0.05 and x indicates not significantly different. In (A), (B), (E), and (F), data are means ± SEM from three independent experiments. In (C) and (D), data are means ± SD from three biological replicates. In (E), *P < 0.05 comparing maximal cytotoxicity in CoA-treated versus untreated conditions for each line, Student's t test. In (F), *P < 0.05, one-way ANOVA with posthoc Tukey test.

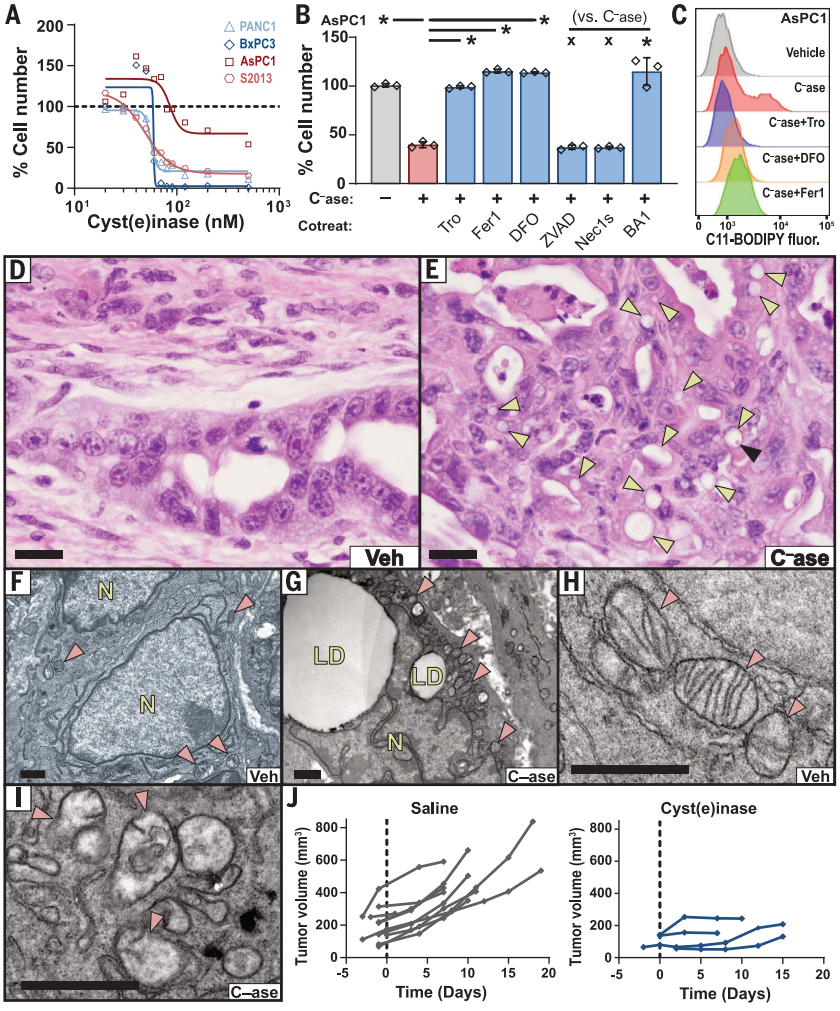

Fig. 4. Cyst(e)inase treatment induces tumor-selective ferroptosis in KPC mice. (**A**) Viability of human PDAC lines cultured with varying concentrations of cyst(e)inase for 48 hours (AsPC1) or 72 hours (PANC-1, BxPC3, and S2-013). (**B**) Viability of AsPC1 cells treated with 90 nM cyst(e)inase (C⁻ase) for 72 hours, alone or in combination with indicated agents, under conditions described in Fig. 1C. (**C**) C11-BODIPY fluorescence was measured by flow cytometry in AsPC-1 cells after 24 hours of treatment with 90 nM cyst(e)inase, alone or in combination with indicated agents, under conditions described in Fig. 1C. (**D** and **E**) H&E-stained sections of pancreatic tumors from KPC mice treated with vehicle or cyst(e)inase. Yellow arrowheads indicate lipid droplets; black arrowhead indicates megamitochondrion; scale bars, 20 μm. (**F** to **I**) TEM of pancreatic tumors from the KPC model treated with vehicle [(F) and (H)] or cyst(e)inase [(G) and (I)]. Red arrowheads indicate mitochondria; LD, lipid droplets; N, nucleus; scale bars, 1 μm. (**J**) Tumor growth curves from KPC mice treated with saline (historical controls) or 100 mg/kg cyst(e)inase, every other day, intraperitoneally. For (A) and (B), data depict mean of three biological replicates. *$P < 0.05$; x, not significant.

were treated with high-dose cyst(e)inase, and their tumor growth was monitored by ultrasound. Notably, all four tumors exhibited stabilizations or regressions, whereas historical vehicle-treated controls never stabilized (Fig. 4J). Thus, we conclude that the therapeutic depletion of cysteine (cystine) can induce ferroptosis in Kras/p53 mutant pancreatic tumors in mice.

In summary, our data add to a growing body of evidence showing that certain cancers, including PDAC, rely on cysteine metabolism to avert ferroptosis. Previously, *SLC7A11* deletion via CRISPR-Cas9 was shown to induce ferroptosis in cultured PDAC cells and slow xenograft engraftment and growth (*18*), and system x_C^- inhibition was shown to limit the growth of lymphoma xenografts, inducing a lipid oxidative signature and other indicators of ferroptosis (*15*). However, cysteine depletion in a PDAC xenograft model had little effect on tumor growth (*19*), perhaps indicating that the nutrient-deprived, hypoxic microenvironment of autochthonous pancreatic tumors may contribute to the tumor-selective cysteine dependency we observed in genetically engineered mouse models of PDAC. Although it is not yet known whether human PDAC is also susceptible to ferroptosis from cysteine depletion, the clinical development of cyst(e)inase for treatment of the metabolic disorder cystinuria provides a pathway for future translation of this concept.

REFERENCES AND NOTES

1. G. M. DeNicola *et al.*, *Nature* **475**, 106–109 (2011).
2. H. Sato *et al.*, *J. Biol. Chem.* **280**, 37423–37429 (2005).
3. W. S. Yang *et al.*, *Cell* **156**, 317–331 (2014).
4. S. J. Dixon *et al.*, *Cell* **149**, 1060–1072 (2012).
5. M. Gao *et al.*, *Cell Res.* **26**, 1021–1032 (2016).
6. J. P. Friedmann Angeli *et al.*, *Nat. Cell Biol.* **16**, 1180–1191 (2014).
7. S. R. Hingorani *et al.*, *Cancer Cell* **7**, 469–483 (2005).
8. S. A. Sastra, K. P. Olive, *Methods Mol. Biol.* **980**, 249–266 (2013).
9. M. Gao *et al.*, *Mol. Cell* **73**, 354–363.e3 (2019).
10. S. J. Dixon *et al.*, *eLife* **3**, e02523 (2014).
11. I. S. Harris *et al.*, *Cell Metab.* **29**, 1166–1181.e6 (2019).
12. K. Shimada *et al.*, *Nat. Chem. Biol.* **12**, 497–503 (2016).
13. J. I. Leu, M. E. Murphy, D. L. George, *Proc. Natl. Acad. Sci. U.S.A.* **116**, 8390–8396 (2019).
14. B. Srinivasan *et al.*, *Nat. Chem. Biol.* **11**, 784–792 (2015).
15. Y. Zhang *et al.*, *Cell Chem. Biol.* **26**, 623–633e9 (2019).
16. K. P. Olive *et al.*, *Science* **324**, 1457–1461 (2009).
17. S. L. Cramer *et al.*, *Nat. Med.* **23**, 120–127 (2017).
18. B. Daher *et al.*, *Cancer Res.* **79**, 3877–3890 (2019).
19. S. Kshattry *et al.*, *NPJ Precis. Onc.* **3**, 16 (2019).

ACKNOWLEDGMENTS

We thank members of the Olive, Lyssiotis, and Stockwell laboratories for technical advice and thoughtful critiques. We also thank K. L. Olive for manuscript editing and S. W. Novak for advice on electron microscopy interpretation. **Funding:** This work was supported by the NIH/NCI Cancer Center Support Grant P30CA013696 and utilized the Confocal and Specialized Microscopy, Molecular Pathology, Flow Cytometry Core, and OPTIC shared resources. M.A.B. was supported by a training grant (T32 A009503) and a predoctoral fellowship (F31 CA180738). D.M.K. was supported by a Department of Education GAANN fellowship through the University of Michigan Program in Chemical Biology. K.P.O. was supported by the Lustgarten Foundation for Pancreatic Cancer Research (2011 Innovator Award) and the NIH/NCI (1R01CA215607). C.A.L. was supported by a Pancreatic Cancer Action Network/AACR Pathway to Leadership award (13-70-25-LYSS), a Dale F. Frey Award for Breakthrough Scientists from the Damon Runyon Cancer Research Foundation (DFS-09-14), a Junior Scholar Award from The V Foundation for Cancer Research (V2016-009), a Kimmel Scholar Award from the Sidney Kimmel Foundation for Cancer Research (SKF-16-005), and NIH grant U24-DK097153. V.P. was supported by a PRCRP Horizon award by the Department of Defense (W81XWH-17-1-0497). L.R.A. and U.M. were supported by NCI CCSG (CA014195) and the Waitt Foundation. B.R.S. is supported by the NCI/NIH (R35CA209896 and P01CA087497). G.M.W. and K.E.D. were funded by a Cancer Center Core Grant (CA014195), the NIH/NCI (R35 CA197687), and funding from the Freeberg Foundation and the Hirschberg Foundation. K.E.D. was also funded by the Salk Women and Special Science Award. **Author contributions:** M.A.B. and K.P.O. conceived and supervised the overall project; M.A.B., D.M.K., I.R.S., A.M., J.K., C.E.M.F., A.R.D., T.H., and T.L. performed in vitro studies with supervision from C.A.L., W.G., B.R.S., and K.P.O.; M.A.B., S.A.S., and C.F.P. performed in vivo studies; D.M.K., V.P., H.-J.L., P.S., L.Z., and Z.P.T. performed and analyzed mass spectrometry studies with supervision from C.A.L.; H.C.M. performed computation analyses; K.E.D. and L.R.A. performed and analyzed the electron microscopy data with supervision from U.M. and G.M.W.; E.S.S. generated the Pdx1-FlpO strain; C.L. generated the cyst(e)inase reagent with supervision from G.G. and E.S.; B.R.S. provided erastin analog material; A.I. and K.P.O. performed pathology analyses; and M.A.B. and K.P.O. wrote the manuscript and drafted the figures with input from all authors. **Competing interests:** B.R.S. holds equity in and serves as a consultant to Inzen Therapeutics and is an inventor on patents and applications related to ferroptosis, including the following U.S. patents and corresponding applications and patents in other countries, all submitted by Columbia University: 10,259,775, 10,233,171, 9,580,398, 20190292135, 20190135782, 20170233370, 20160297748, 20150079035, 20080299076, 9,938,245, 20160332974, 9,695,133, 20150175558, 8,546,421, 20100081654, 8,535,897, 20110008803, 8,518,959, 20090214465, 8,124,365, 7,358,262, 20080220454, 7,615,554, 20190315681, and 20070161644. G.G. and E.S. have an equity interest in Aeglea Biotherapeutics, a company

that has licensed the commercial development of Cyst(e)inase, and are inventors on U.S. patents and corresponding applications and patents in other countries, all submitted by the University of Texas, related to L-cyst(e)inase: 10,363,311 and 20180327734. The other authors declare no competing interests, financial or otherwise. **Data and materials availability:** Cyst(e)inase is available from G.G. and E.S. under a material transfer agreement with the University of Texas. RNA sequencing datasets are available at Gene Expression Omnibus (accession no. GSE119628). All other data are available in the text or the supplementary materials. Mouse strains comprising the KPC and KPFSR models (other than Pdx1-FlpO) were provided through material transfer agreements with EUCOMM ($Slc7a11^{Flox}$), Univ. Cincinnati (Pdx1Cre), and MIT (all others).

SUPPLEMENTARY MATERIALS

science.sciencemag.org/content/368/6486/85/suppl/DC1
Materials and Methods
Figs. S1 to S13
Table S1
References (*20*–*43*)
Movies S1 to S3

View/request a protocol for this paper from *Bio-protocol*.

13 February 2019; resubmitted 25 October 2019
Accepted 8 March 2020
10.1126/science.aaw9872